Published in final edited form as:
J Comp Neurol. 2006 June 10; 496(5): 706–722.

Subpopulations of Neurons Expressing Parvalbumin in the Human Amygdala

HARRY PANTAZOPOULOS[1], **NICHOLAS LANGE**[2,3,4], **LINDA HASSINGER**[1], and **SABINA BERRETTA**[1,2,*]

1*Translational Neuroscience Laboratory, McLean Hospital, Belmont, Massachusetts 02478*

2*Department of Psychiatry, Harvard Medical School, Boston, Massachusetts 02115*

3*Department of Biostatistics, Harvard School of Public Health, Boston, Massachusetts 02115*

4*Neurostatistics Laboratory, McLean Hospital, Belmont, Massachusetts 02478*

Abstract

Amygdalar intrinsic inhibitory networks comprise several subpopulations of γ–aminobutyric acidergic neurons, each characterized by distinct morphological features and clusters of functionally relevant neurochemical markers. In rodents, the calcium-binding proteins parvalbumin (PVB) and calbindin D28k (CB) are coexpressed in large subpopulations of amygdalar interneurons. PVB-immunoreactive (-IR) neurons have also been shown to be ensheathed by perineuronal nets (PNN), extracellular matrix envelopes believed to affect ionic homeostasis and synaptic plasticity. We tested the hypothesis that differential expression of these three markers may define distinct neuronal subpopulations within the human amygdala. Toward this end, triple-fluorescent labeling using antisera raised against PVB and CB as well as biotinylated *Wisteria floribunda* lectin for detection of PNN was combined with confocal microscopy. Among the 1,779 PVB-IR neurons counted, 18% also expressed CB, 31% were ensheathed in PNN, and 7% expressed both CB and PNN. Forty-four percent of PVB-IR neurons did not colocalize with either CB or PNN. The distribution of each of these neuronal subgroups showed substantial rostrocaudal gradients. Furthermore, distinct morphological features were found to characterize each neuronal subgroup. In particular, significant differences relative to the distribution and morphology were detected between PVB-IR neurons expressing CB and PVB-IR neurons wrapped in PNNs. These results indicate that amygdalar PVB-IR neurons can be subdivided into at least four different subgroups, each characterized by a specific neurochemical profile, morphological characteristics, and three-dimensional distribution. Such properties suggest that each of these neuronal subpopulations may play a specific role within the intrinsic circuitry of the amygdala.

Keywords

calbindin D28k; perineuronal nets; immunocytochemistry; confocal microscopy; basolateral complex of the amygdala

The basolateral complex of the amygdala (lateral, basolateral, and accessory basal nuclei; BLC) plays an important role in assigning affective and motivational significance to sensory inputs, forming emotional memories, and generating emotional responses (Gloor, 1986;Halgren, 1992;Brothers, 1990;LeDoux, 1992;Aggleton, 1993;Adolphs et al., 1994). Complex intrinsic inhibitory circuits are believed to represent a critical component of the neural networks

*Correspondence to: Sabina Berretta, MRC3, McLean Hospital, 115 Mill Street, Belmont, MA 02478. E-mail: s.berretta@mclean.harvard.edu

underlying these functions. Among the several subpopulations of interneurons forming these circuits, those expressing the calcium-binding protein parvalbumin (PVB) are localized preferentially within the BLC (Sorvari et al., 1995). These neurons have been shown to affect information processing in this region crucially. For instance, the extremely low spontaneous firing rates typical of BLC projection neurons are thought to be the result of strong intrinsic inhibitory pressures originating from PVB-immunoreactive (-IR) neurons (Rainnie et al., 1991;Paré and Gaudreau, 1996). Furthermore, interactions between fast-firing interneurons, putatively expressing PVB, and projection neurons have been suggested to be involved in generating rhythmic oscillatory activity in the BLC (Paré and Gaudreau, 1996 Pape et al., 1998;Paré et al., 2002;Muller et al., 2005).

The specific pattern of connectivity, cytoarchitectonics, and neurochemical profile of PVB-IR neurons underlies their functional specialization. Similar to other brain regions, PVB-IR neurons in the BLC are classic chandelier and basket cells and use γ-aminobutyric acid (GABA) as their main neurotransmitter (Kemppainen and Pitkanen, 2000;McDonald and Betette, 2001;McDonald and Mascagni, 2001). Their terminals form axoaxonic cartridges and perisomatic basket-like plexus (Pitkanen and Kemppainen, 2002) and principally innervate projection neurons (Sorvari et al., 1996a). Such a synaptic arrangement suggests a powerful inhibitory control of PVB-IR neurons over projection neurons within the BLC (Smith et al., 1998). In turn, these neurons are thought to receive their main inputs from amygdalar projection neurons, thus creating a powerful inhibitory feedback loop (Smith et al., 2000).

The neurochemical profile of these neurons has a profound effect on their physiological properties. PVB is a member of the EF-hand family of calcium-binding proteins and, as such, acts as a buffer regulating Ca^{2+} homeostasis. By affecting Ca^{2+} transients, calcium-binding proteins participate in broad range of functions, such as excitability, synaptic plasticity, neurotransmitter release, gene expression, neuroprotection, and growth (Berridge, 1998;Vreugdenhil et al., 2003). The specific characteristics of PVB in terms of its affinity for Ca^{2+} and Mg^{2+} ions, and its kinetics for binding and releasing Ca^{2+}, make it a “slow” Ca^{2+} buffer (Chard et al., 1993;Caillard et al., 2000;Lee et al., 2000;Schwaller et al., 2002). Growing evidence suggests that these properties may account for the specialized role that PVB-IR neurons play in functions such as short-term synaptic plasticity and the shaping of population patterns of activity (Freund and Buzsaki, 1996;Caillard et al., 2000). Other molecules preferentially expressed by these neurons are also involved in such specific functions. For instance, expression of the alpha 1subunit of the $GABA_A$ receptor in amygdalar PVB-IR neurons confers on these receptors specific kinetic properties that may be important for oscillatory activity (McDonald and Mascagni, 2004), and the Kv3.1b subunit of voltagegated potassium channels has been proposed to be necessary for the generation of the high firing rates typical of these neurons (Perney et al., 1992;Lenz et al., 1994;Weiser et al., 1995;Gan and Kaczmarek, 1998).

In the rodent and primate BLC, PVB-IR neurons are neurochemically and morphologically heterogeneous. Morphologically, large multipolar, fusiform, and small round cells have been described (Sorvari et al., 1995). Among the various neurochemical markers coexpressed in PVB-IR neurons, the calcium-binding protein calbidin D28k (CB) appears to be one of the most common. In rodents, approximately 80% of all amygdalar PVB-IR neurons also express CB (McDonald and Betette, 2001). Investigations in monkeys and humans suggest a more moderate overlap (Hartig et al., 1995;Sorvari et al., 1996b;Pitkanen and Kemppainen, 2002). Colocalization of PVB and CB in the human amygdala has been examined in the present study for the first time.

PVB-IR neurons have also been found to be frequently ensheathed by perineuronal nets (PNN; Celio, 1993;Hartig et al., 1995;Seeger et al., 1996;Morris and Henderson, 2000). These nets

are lattice-like coatings found to wrap around the somata and proximal dendrites of specific types of neurons (Bignami et al., 1992;Bruckner et al., 1993;Celio and Blumcke, 1994;Celio et al., 1998). They are composed mainly of extracellular matrix chondroitin sulfate proteoglycans (Celio and Blumcke, 1994) and can be detected by using N-acetylgalactosamine-specific lectins such as *Wisteria floribunda* lectin (Hartig et al., 1992, 1994). In this study, we will refer to structures labeled using *Wisteria floribunda* lectin as *PNN*. The specific composition of PNN varies for distinct neuronal subpopulations with which they are associated (Lander et al., 1997), suggesting specialized functional properties. In general, PNN are believed to be involved in maintenance of ionic homeostasis, neuroprotective functions, and synaptic plasticity (e.g., Murakami and Ohtsuka, 2003;Morawski et al., 2004;Rhodes and Fawcett, 2004). The frequent association between PVB-IR neurons and PNN (Celio, 1993;Seeger et al., 1996;Morris and Henderson, 2000) suggests that the latter may be necessary to support some of the functions of PVB-IR neurons.

The main goal of this study was to investigate whether distinct subpopulations of PVB-IR neurons in the human amygdala can be distinguished on the basis of their colocalization with CB and PNN. Using triple-fluorescent immunolabeling in combination with light and confocal microscopy, we examined the distribution and colocalization of PVB, CB, and PNN as well as the morphological characteristics associated with these markers. These results indicate that at least four subgroups of PVB-IR neurons can be distinguished on the basis of their expression of CB and/or PNN. Each subgroup shows distinct morphological features and rostrocaudal distributions.

MATERIALS AND METHODS

Human subjects and tissue processing

Tissue blocks, each containing the whole amygdala from a normal donor (n=5), were obtained from the Harvard Brain Tissue Resource Center (Table 1). The blocks were stored in 0.1 M phosphate buffer (PB; pH 7.4) containing 4% paraformaldehyde, 0.1% Na azide (pH 7.4) for 2 weeks, followed by 1 week in cryoprotectant solution (30% glycerol, 30% ethylene glycol, 0.1% NaAzide in PB; pH 7.4) at 4°C. Blocks were then cut into sequential 3-mm coronal slabs with an antithetic tissue slicer and resectioned into 40-μm serial sections on a freezing microtome (860; American Optical, Buffalo, NY). Sections were stored in the same cryoprotectant solution at –20°C. Tissue from several regions from each brain was analyzed by a neuropa-thologist to determine any evidence of gross and/or macroscopic changes consistent with Alzheimer's disease, cerebrovascular accident, ethanol abuse, or other confounding factors. A psychiatrist examined all medical records to confirm that subjects were free of any psychiatric illness.

Immunocytochemical procedures

Monoclonal anti-PVB antibody (P3088, lot 10K4846; clone PARV-19, ascites fluids; Sigma-Aldrich, St. Louis, MO) is derived from the PARV-19 hybridoma produced by the fusion of mouse myeloma cells and splenocytes from an immunized mouse. Purified frog muscle parvalbumin was used as the immunogen. This antibody has been found to react with parvalbumin (12 kDa) from human, bovine, goat, pig, rabbit, dog, cat, rat, frog, and fish. It does not react with other members of the EF-hand family of calcium-binding proteins. Immunoblot characterization showed a single band corresponding to 12 kD (information kindly provided by Sigma-Aldrich). Anti-CB affinity-isolated antibody (C7354, lot 013K4875; Sigma-Aldrich) was produced in rabbit. The immunogen was a synthetic peptide corresponding to the C-terminal region of rat CB (amino acids 185–199). This sequence is identical in the corresponding human CB sequence, but it is not found in other members of the EF-hand family. Immunoblot characterization showed a single band corresponding to 28 kD. Preabsorption with

the synthetic peptide resulted in complete blockade (information kindly provided by Sigma-Aldrich). PNNs were labeled using biotinylated *Wisteria floribunda* lectin (molecular weight 116,000 –125,000), a glycoprotein isolated from seeds of *Wisteria floribunda*. This lectin binds to carbohydrate structures terminating in N-acetylgalactosamine, which, unlike other extracellular matrix molecules, are associated specifically with PNNs (Hartig et al., 1992;Celio et al., 1998).

For triple fluorescent labeling of PVB, CB, and PNN, immunocytochemistry with specific primary antisera raised against PVB and CB and secondary antisera conjugated with nonoverlapping fluorescent markers was combined with histochemical detection of PNN with biotinylated *Wisteria floribunda* lectin and streptavidin-conjugated with a third, nonoverlapping, fluorescent marker. Free-floating sections were washed in 0.01 M PB 0.9% NaCl (PBS; pH 7.4) and then boiled in 1:100 Antigen Unmasking solution (Vector, Burlingame, CA) in PBS (pH 7.0) for 3 minutes to reveal the antigens and thus facilitate their binding to the primary antisera. Solutions for all the following steps were made in PBS with 0.5% Triton X (PBS-Tx; pH 7.4). Each step was followed by washes in the same solution. Sections were incubated in 5% bovine albumin serum (1 hr) and placed in a cocktail of primary antisera raised in mouse against PVB (1:10,000) and in rabbit against CB (1:10,000; Sigma-Aldrich) in 1% bovine albumin serum at 4°C for 72 hr. Sections were then incubated (2 hr) with a cocktail containing Alexa Fluor horse anti-mouse (1:250; wavelength 555) and Alexa Fluor goat anti-rabbit (1:250; wavelength 647) for 4 hr. The third labeling, i.e., PNNs, was then obtained by placing the sections in biotinylated *Wisteria floribunda* lectin (1:500; Vector) in 1% bovine albumin serum for 24 hr at 4°C followed by 4 hr incubation in Alexa Fluor streptavidin (1:2,000; wavelength 488). Finally, sections were incubated in 1 mM $CuSO_4$ (pH 5.0) for 10 minutes to eliminatelipofuscin autofluorescence (Schnell et al., 1999). After mounting on gel-coated slides, sections were incubated for 3 minutes with blue-fluorescent Nissl stain (1:100 in PBS; wavelength 435) and coverslipped with GelMount (Biomeda Corp., Foster City, CA). All fluorescent probes were purchased from Molecular Probes (Eugene, OR).

To test the adequacy of the protocol described above, we carried out a pilot study with a small subsample of sections. Single fluorescent labeling for each of the three markers used (PVB, CB, *Wisteria floribunda* lectin) was compared with three different triple-staining protocols to test for loss of labeling potentially caused by factors such as sequence of the incubations in each of the antisera.

Protocols for single fluorescent staining for each of the three markers were identical to those described above. In brief, three different sets of sections were incubated in Antigen Unmasking solution (Vector), bovine albumin serum, and then primary antibody for either PVB or CB (as described above) or in biotinylated *Wisteria floribunda* lectin (PNN). Detection of the antigens was obtained by incubation in Alexa Fluor (555) horse anti-mouse (1:250; PVB) or Alexa Fluor (647) goat anti-rabbit (1:250; CB) or Alexa Fluor streptavidin (488; 1:2,000). Labeled IR neurons in each section were counted using confocal microscopy. The numbers of neurons counted on single-labeled sections for each of the three markers matched virtually perfectly those obtained with the triple fluorescent protocol described above, which was thus selected for this study. On the other hand, two other triple fluorescent protocols, similar to the one described above except for the sequence of incubations in primary and secondary antisera, were rejected because the numbers of neurons counted were at least 10% lower than those obtained with the single labeling protocols.

For further confirmation of the reliability of colocalization between PVB-IR neurons and PNNs, dual-color diaminobenzidine (DAB) labeling of a small subsample of sections was combined with light microscopy as previously described in detail (see Fig. 2L; Berretta et al., 1997). In brief, antigen unmasking procedures as described above were followed by incubation

in 0.3% H_2O_2 and 10% EtOH and 2% bovine albumin serum, all in PBS-Tx. Sections were then successively incubated in primary antibody raised in mouse against PVB (1:10,000; Sigma-Aldrich), horse anti-mouse biotinylated secondary antiserum (Vector), and streptavidin (Zymed, South San Francisco, CA). Nickel-enhanced DAB/peroxidase complex was used for detection (purple-black reaction product). Following blocking steps with 0.3% H_2O_2, 0.6% avidin/biotin (Blocking Kit; Vector), and 2% bovine albumin serum, sections were incubated with biotinylated *Wisteria floribunda* lectin (1: 500; Vector). DAB in Na^+ cacodylate buffer (pH 7.0) was used for PNN detection (brown reaction product). We used these stainings to confirm qualitatively the distribution and morphology of PVB-IR neurons and PNNs and their coexpression (see Fig. 2L).

Light microscopy analysis showed that the distribution patterns of PVB, CB, and PNNs staining in our tissue correspond well to those detected in the human and monkey amygdala and entorhinal cortex in other laboratories (Hartig et al., 1995;Sorvari et al., 1995,1996b;Mikkonen et al., 1997). Standard tests for antisera specificity included omission of either the primary or the secondary antisera. No labeling was detected in any of these trials.

Data collection

Four representative sections were selected from each subject, matched between subjects for rostral-caudal level (Fig. 1), and processed for triple fluorescent labeling for PVB, CB, and PNN as described above. For the purpose of these analyses, data collection was restricted to the lateral (LN), basal (BN), accessory basal (AB), and cortical (CO) nuclei of the amygdala (BLC-CO; Fig. 1), where PVB-IR neurons in the amygdala are selectively located (Sorvari et al., 1995). We refer to the two rostral sections (1 and 2) as to the rostral portion of the BLC-CO and to the two caudal sections as to its caudal portion. It should be noted that these sections were chosen to maximize the number of PVB-IR neurons counted and to obtain a reliable sample of these neurons. For this reason, the most rostral and caudal poles of the BLC-CO, where these neurons are represented rather sparsely, were not included in the analysis.

A Leica Confocal Microscope System equipped with TRITC, FITC, and CY5 filters and a Zeiss Axioscope 2 Plus microscope equipped with TRITC, FITC, CY5, and DAPI filters were used for this study. In a first step, quantitative analysis of triple-labeled sections was performed with a Leica Confocal Microscope System. This system allows scanning through the Z axis of each section in small increments, enabling us to resolve among two or more neurons sharing the same Y and X (but not Z) coordinates. For this analysis, the LN, BN, AB, and CO were combined in one region (BLC-CO), because under confocal microscopy it was not possible to distinguish the borders between them accurately. However, for one amygdala in which a particular set of landmarks made it possible to reliably draw the borders of the lateral and basal nuclei, we were able to collect data from these nuclei individually. Using a ×40 objective, the BLC-CO (or LN and BN) was scanned systematically in its whole dorsoventral and lateromedial extent with 1-μm increments throughout the Z-axis so that *all* IR neurons in this region could be recorded. Filters used were TRITC 555 (PVB), FITC 488 (PNN), and CY5 647 (CB; Fig. 2). Every IR neuronal profile was recorded for its expression of any or all of the three markers (PVB, CB, and *Wisteria floribunda* lectin as a marker for PNN; Fig. 2). Colocalization of two or more markers was established when the respective fluorescence signal was clearly present at the same range within the Z-axis for each of the markers examined and confirmed by a color change of overlapping markers (Fig. 2D,H). IR neurons identified through confocal images were also classified in terms of their morphological characteristics into large and small multipolar cells (LM, SM) and large and small bipolar cells (LB, SB). Multipolar cells were defined as having spherical or irregularly shaped somata from which three or more primary dendrites emerge. Within this category, cells were labeled as large or small depending on whether the somata cross-sectional area was more or less than 150 μm^2, respectively (Fig.

3A,B). Neurons were classified as bipolar when they had fusiform somata with dendrites emerging from the two opposite poles (Fig. 3C,D). These neurons were considered “large” if their somata cross-sectional area was more than 120 3m. This classification represents only a slight modification with respect to that proposed by Sorvari et al. (1995) and is based on our observations on the size and shape of PVB-and CB-IR neurons in the human amygdala. Cross-sectional area for all neurons examined was measured by using the Leica TCS Confocal System, which allows tracing around neuron somata.

As a second step, qualitative analysis of the distribution of labeled neurons within BLC-CO subdivisions was carried out with a Zeiss Axioscope 2 Plus microscope equipped with TRITC, FITC, and CY5 filters, as well as a DAPI filter, which enabled us to detect the blue-fluorescent Nissl stain. Using the latter filter and a ×4 objective, the borders of the LN, BN, AB, and CO were outlined according to cytoarchitectonic characteristics (Amaral et al., 1992;Sorvari et al., 1995;Gloor, 1997). The distribution of each neuronal subgroup identified within each of these nuclei was examined using a ×10 objective. The LN was further subdivided into lateral, ventrolateral, and medial subdivisions and the BN into magnocellular, intermediate, and parvicellular subdivisions. All anatomical subdivisions were also confirmed with light microscopy in adjacent sections immunostained for PVB and Nissl stained with cresyl violet. The nomenclature adopted was that used by Sorvari et al. (1995). Cytoarchi-tectonic criteria for identification of amygdala subregions in Nissl-stained sections were derived from those described by Amaral et al. (1992) and Sims and Williams (1990).

Statistical analysis

The number of neurons provided in our data and figures represents the number of neurons in the four sections analyzed. The main outcome measure was the number of cells counted for each neuronal subtype. We did not attempt to estimate total number of IR neurons in the BLC-CO because of the necessity for a relatively sparse sampling scheme (i.e., four sections/subject) and the presence of strong rostrocaudal distribution gradients. Instead, we chose to match carefully the rostrocaudal level for each section between subjects to allow reliable grouped comparisons. Because data were not normally distributed, a logarithmic transformation was applied. A preliminary repeated-measures mixed-effects ANOVA was employed, followed by a pooled analysis across sections for all five cases to calculate percentage representation of each category of PVB-IR neurons. To compare the rostrocaudal distribution of each of the subtypes of neurons identified, we first reduced the log counts across sections to estimated linear slopes. Paired *t*-tests on rostrocaudal slopes from each case were used for comparisons of neuronal subtypes (see Table 2). Conservative Bonferroni corrections were employed for correlated multiple comparisons. Chi-square analyses were used to test the hypothesis that specific neurochemical subpopulations may correspond to distinct morphological subtypes. The statistical software used for all analyses was S-Plus (Insightful Corp., Seattle, WA) and JMP v5.0.1a (SAS Institute Inc., Cary, NC). All graphs were created in Microsoft Excel 2004 v.11.1 (Microsoft Corp., Redmond, WA). Photomicrographs were processed in Adobe Photoshop 7.0 and Adobe Illustrator 10 (Adobe Systems Inc., San Jose, CA). Contrast and brightness were modified up to 10% of the original values.

RESULTS

PVB-IR neurons

In total, 1,779 PVB-IR neurons were counted in the BLC-CO of five normal brain donors (four sections/case).No statistically significant differences relative to numbers of PVB-IR neurons per case were detected among subjects using ANOVA ($F = 0.1914$, $P = 0.667$). The somata and dendrites of IR neurons were generally intensely immunostained (Figs. 2A,E,I, 3A,C, 4). Descriptively, PVB-IR neurons appeared to be localized preferentially in the LN, primarily in

its lateral and ventrolateral subdivisions and, to a lesser extent, in the magnocellular subdivision of the BN (Fig. 4). PVB-IR neurons increased gradually from the rostral pole of the amygdala, where they were only very sparsely represented, and reached their peak toward the middle to caudal one-third of this nucleus (Fig. 4). A decrease was again noted toward the caudal pole where much fewer PVB-IR neurons were detected. Numerous IR fibers were also visible, with the highest densities in the LN and BN (Fig. 4, inset). In these nuclei, IR puncta were often found to surround unstained somata or to align in "cartridge" formations. These distribution patterns are consistent with those observed in a recent light microscopy study from our laboratory (Berretta et al., manuscript in preparation) and those reported by Sorvari et al. (1995). As also described by the same group, PVB-IR neurons in the amygdala were found to be cytoarchitectonically heterogenous. Intense IR was detected in small multipolar cells (SM), large multipolar cells (LM), small bipolar cells (SB), and large bipolar cells (LB).

CB-IR neurons

In total, 816 CB-IR somata were counted. IR somata were most numerous in the AB nucleus, while large numbers were also detected in the CO nucleus (Fig. 4). Low to moderate numbers of these neurons were localized in the LN and BN, primarily in the medial and parvicellular subdivisions, respectively (Fig. 4). Similar to PVB-IR neurons, CB-IR cells have also been shown to be morphologically heterogeneous, with small and large multipolar neurons representing the most numerous groups (Sorvari et al., 1996b). In this study, all neurons displaying IR for CB, but not the other two markers, were grouped under the general category of "multipolar" because of the technical limitations relative to the immunofluorescent labeling, which did not allow us to visualize clearly the thin dendrites that characterize these neurons on the basis of the CB-IR alone (Sorvari et al., 1996b). Particularly large neurons with more intense dendritic IR were labeled as LM (Fig. 4, inset).

PNN

In total, 1,056 PNNs were counted over the BLC-CO of five subjects (four sections/subjects). The morphology and size of the majority of the PNNs in this region suggest that they surround LM neurons (Figs. 2B,L, 4, inset), although SM, SB, and LB cells were also found to have PNNs. PNNs were found mainly in the LN and BN. This distribution is reminiscent of that reported in nonhuman primates (Har-tig et al., 1995). PNNs were concentrated primarily in the lateral and ventral divisions of the LN and magnocellular division of the BN. Sparse PNN were also detected in the other divisions of the BLC-CO. The number of PNN increased along the rostrocaudal axis of the BLC-CO.

Neurochemically distinct PVB-IR neuron subgroups

PVB-IR neurons were classified into four distinct subgroups on the basis of their expression of CB and PNN (Fig. 5A). Of 1,779 PVB-IR neurons counted, 44.0% did not express either CB or PNN (PVB/–/–), 31.4% were ensheathed by PNN but did not express CB (PVB/PNN/–), 17.5% expressed CB but did not have PNN (PVB/–/CB), and only 6.9% were labeled with both CB and PNN (PVB/ PNN/CB). Examples of these neurons are shown in Figure 2.

Distributions of PVB-IR neuron subgroups within the BLC-CO

Percentages relative to each neuronal group varied along the rostrocaudal axis of the BLC-CO (Fig. 6A,B). For instance, in the caudal portion (sections 3– 4; Fig. 6B) of BLC-CO, 39.6% of all PVB-IR neurons were PVB/PNN/–, whereas, in the rostral portion (sections 1–2; Fig. 6A), this percentage fell to 23.2%. In contrast, percentages of PVB/–/CB neurons were higher in the rostral portion (23.7%) in comparison with the caudal one (11.4%; Fig. 6 A,B).

A preliminary repeated-measures mixed-effects ANOVA revealed strong ($P<<0.05$) yet differing linear effects across sections for all neuronal subtypes except for the PVB/–/CB and PVB/PNN/CB combinations (Fig. 7), indicating that a subsequent, more detailed analysis of slope differences for all pairwise comparisons of subtypes is well founded. Paired *t*-test analysis of the rostrocaudal distribution slopes of each neuronal subpopulation showed significant differences between PVB/PNN/– and PVB/–/CB (P =0.04) but not between other groups (Table 2, Fig. 8A). It is important to note that rostral to caudal distributions did not vary significantly between subjects.

In one representative amygdala, a second count of each neuronal subpopulation was taken separately from the LN and BN (Fig. 9). In the LN, the rostrocaudal distribution of each neuronal subpopulation was found to be strikingly similar to that shown in the BLC-CO (compare Fig. 9, upper panel, with Fig. 7). Distributions in the BN appear to vary to a much lesser degree (Fig. 9, lower panel).

Percentage differences along the rostrocaudal axis were reflected in changes in numbers of neurons in each population. Significant increases of PVB/–/– (P=0.04), PVB/ PNN/– (P=0.001), –/–/CB (P=0.04), and –/PNN/– (P=0.006) neurons were detected in the caudal portion of the BLC-CO compared with the rostral one (Fig. 6C). Conversely, PVB/–/CB neurons were slightly decreased in the caudal portion. These changes also involved greater differences between groups in the caudal portion, as demonstrated by comparisons between pairs of neuronal groups (paired *t*-test corrected for multiple comparisons), which were not significant in the rostral half of the BLC-CO, while several significant differences were detected in the caudal half (Table 3).

Fluorescent Nissl staining (DAPI filter) was used to determine, qualitatively, the distribution of each PVB-IR neuronal subgroup within the LN, BN, ABN, and CO (Fig. 10). Most of the PVB/PNN/– neurons were detected in the LN, particularly in its ventrolateral subdivision, and in the magnocellular subdivision of the BN (Fig. 10). Very sparse PVB/PNN/– neurons were also detected in the other subdivisions of the LN and BN, with the exception of the parvicellular subdivision of the BN, which was virtually devoid of this neuronal subgroup. No PVB/PNN/– neurons were detected in the AB or CO. PVB/PNN/CB neurons showed a very similar distribution. In contrast, the PVB/–/CB neurons were found mainly in the lateral and medial divisions of the LN, particularly rostrally (Fig. 10). Fewer PVB/–/CB neurons were observed in the magnocellular and intermediate divisions of the BN, as well as the ventrolateral LN, and even lower numbers were detected in the AB and CO.

Morphological characteristics of neuronal subpopulations

A Chi-square analysis showed that each neurochemical subpopulation investigated is characterized by specific morphological features (χ^2 = 186.4; P= 0.0001; Fig. 11). PVB/–/– neurons represented a heterogenous group consisting of four morphological subtypes (LM, SM, SB, and LB). All of the other subgroups were more morphologically homogenous: 81.6% of PVB/PNN/– neurons and 68.6% of –/PNN/– neurons were LM cells, whereas the majority of PVB/–/CB neurons (92.3%) and PVB/PNN/CB neurons (91.6%) were SB cells (Fig. 11). As mentioned above, in our material, it was difficult to detect accurately the morphological characteristics of most –/–/CB neurons. For this reason, these neurons are grouped in Figure 11 under the category of “multipolar” cells. Although descriptive observations suggested that these neurons might overall be smaller than those expressing PVB and/or PNN, a smaller group of LM cells was also detected.

DISCUSSION

These results indicate that PVB-IR neurons in the human amygdala can be divided into at least four subgroups on the basis of their expression of CB and PNN. Such subgroups have distinct rostrocaudal distributions and morphological characteristics (Figs. 7, 10, 11). In particular, PVB/PNN/– and PVB/–/CB neuronal subpopulations differed significantly with respect to their prevalence, rostrocaudal distributions, and morphological features. In contrast, PVB/–/– and PVB/PNN/– neurons shared similar features, with the exception of their morphological profiles. We propose that such differences among subgroups of PVB-IR neurons might imply specialized functional roles.

PVB-IR neurons in the BLC, as well as in other cortical and cortical-like regions, are GABAergic and tend to form clusters of synaptic terminals that surround the somata and proximal axon segments of projection neurons (DeFelipe et al., 1989;Hendry et al., 1989;Fonseca et al., 1993;Freund and Buzsaki, 1996;Gabbott and Bacon, 1996;Sorvari et al., 1996a;McDonald and Mascagni, 2001). In the BLC, these neurons have been shown to receive their main inputs from intrinsic projection neurons (Smith et al., 2000;McDonald et al., 2005). These features strongly support the hypothesis that a role for PVB-IR neurons in the BLC may be to exert a powerful control over the activation of projection neurons through a feedback inhibitory loop. Within this general framework we suggest that neurochemically distinct subgroups of PVB-IR neurons might differentially modulate the outflow of information from the BLC depending on their specific physiological properties and location within this nuclear complex.

Relationship between PVB and PNNs in the human amygdala

PVB-IR neurons are the neuronal subpopulation most commonly associated with PNNs (Kosaka and Heizmann, 1989;Luth et al., 1992;Celio, 1993;Hartig et al., 1995;Morawski et al., 2004). Furthermore, at least in the neocortex and hippocampus, PVB-IR neurons ensheathed by PNN have been shown to express Kv3.1b (Sekirnjak et al., 1997;Gan and Kaczmarek, 1998;Hartig et al., 1999), a subunit of voltagegated potassium channels that, like PNNs, has been found to be associated with highly active neurons (Perney et al., 1992; Lenz et al., 1994;Weiser et al., 1995;Gan and Kaczmarek, 1998). PVB-IR neurons are in fact characterized electrophysiologically as “fast-spiking”. This definition includes neurons that display high repetitive firing, short-duration action potentials with short duration afterhyperpolarization, and a small degree of spike frequency adaptation (Kawaguchi and Kubota, 1995;Cauli et al., 1997). Such a “fast-spiking” profile has been specifically shown in PVB-IR neurons ensheathed by PNNs in the medial septum/diagonal band (Morris and Henderson, 2000). Overall, these considerations point to a strong functional association between PVB and PNNs. In fact, it has been suggested that PVB is necessary to create the intracellular environment needed for the fast spiking, nonadaptive activity whereas PNNs form a highly anionic microenvironment that might allow these neurons to sustain such activity by keeping the extracellular space from accumulating an excessive concentration of potassium (Hartig et al., 1999;Morris and Henderson, 2000). In light of the strong association between the presence of PNNs and the fast-spiking properties discussed above, our results suggest that, in the human BLC, a subgroup of neurons, amounting at least to 30 –35% of all PVB-IR cells, might have physiological properties similar to those described as “fast-spiking” in rodents.

Our results also show that, in the human BLC-CO, a substantial subgroup of PVB-IR neurons does not possess PNNs. These neurons were smaller and morphologically heterogeneous, confirming observations in other brain regions (Hartig et al., 1995;Morris and Henderson, 2000). Given the considerations discussed above, it is reasonable to suggest that almost half (44%) of the PVB-IR neuronal population in the human BLC might lack at least some of the electrophysiological characteristics typical of “fast-spiking” neurons. If this is correct, two

equal-sized PVB-IR neuronal populations in the amygdala may display different physiological properties and serve different functional roles. It is interesting to note that the rostrocaudal distributions of PVB/PNN/– and PVB/–/– neurons are similar, suggesting that both of these subgroups might be needed for information processing within the same microcircuitry.

In our study, most of the neurons possessing PNNs were identified morphologically as LM cells (Fig. 11). This observation is consistent with the theory that PNNs may be necessary to provide the cytoskeletal and metabolic support necessary to large, highly active neurons (Celio and Blumcke, 1994). It has been suggested that, while providing such support, PNN may stabilize existing synaptic contacts and prevent the formation of new ones (Hockfield and Kalb, 1993;Celio and Blumcke, 1994;Yamaguchi, 2000;Rhodes and Fawcett, 2004). It is thus possible that neurons wrapped in PNNs, including PVB/PNN/– and PVB/PNN/CB neurons in the human BLC-CO, may have limited synaptic plasticity.

In the present study, approximately 68% of all PNN ensheathed PVB-IR neurons, suggesting that approximately 30% of PNNs in the human BLC-CO are associated with neurons other than those expressing PVB. This estimate is consistent with observations in other brain regions (Wegner et al., 2003). The phenotype of amygdalar –/PNN/– neurons was not investigated in this study. For nonhuman primate amygdala, it was found that all PNNs wrap around glutamic acid decarboxylase-IR neurons (Hartig et al., 1995), suggesting that in this region only GABAergic interneurons possess PNN. However, in our tissue, the morphology of LM –/PNN/– neurons was often strongly reminiscent of that typical of pyramidal neurons (see Fig. 2J). The possibility that at least some of the –/PNN/– neurons in the amygdala may be glutamatergic projection neurons is supported by descriptions of PNN-positive, glutamate-IR pyramidal neurons in the rodent cortex (Wegner et al., 2003). In either case, the strong association between PNNs and “highly active” neurons (Horn et al., 2003) suggests that –/PNN/– neurons might represent a distinct neuronal subpopulation characterized by a high firing rate.

Coexpression of PVB and CB in human amygdala neurons

The present results indicate that, in the human BLC-CO, approximately 25% of PVB-IR neurons also express CB. Conversely, 52% of CB-IR neurons coexpressed PVB. It is important to note that, for the purpose of this study, we limited our measurements to the BLC-CO. In humans, this region contains virtually all of the PVB-IR neurons in the amygdala, whereas CB-IR neurons are less densely represented. These distributions account for the fact that numbers of –/–/CB neurons included in our data are lower than would be expected if the rest of the amygdala nuclei (e.g., central and medial nuclei) were investigated. Furthermore, a possibility common to all immunocytochemical studies is that a portion of amygdala neurons may not be counted if they express one or both markers below detectable levels. Such an occurrence might have had a impact on the proportion of neuronal subgroups reported in this paper. For instance, the numbers of CB-IR neurons counted in the five subjects included in this study appear to be lower than those reported for one subject by Sorvari et al. (1996b). The reasons for this discrepancy are not clear at this time and may be multifold. A higher number of CB-IR neurons might have resulted in higher percentages of PVB-IR neurons expressing CB or simply in higher percentages of –/–/CB neurons.

CB, like PVB, belongs to the EF-hand calcium-binding protein family. However, its Ca^{2+} binding rates and affinities are different from those described for PVB and define it as a “fast” Ca^{2+} buffer (for review see Schwaller et al., 2002). Unlike PVB, CB has been shown to interact with protein and/or subcellular structures, suggesting a possible role in signal transduction or activity-dependent changes of its intracellular mobility (Schwaller et al., 2002). These differences are also reflected in the physiological properties of primate and rodent CB-IR neurons, described as “low-threshold spike cells” (Kawaguchi and Kubota, 1993) or “nonfast-

spiking" cells (Zaitsev et al., 2005), indicating an electrophysiological profile fundamentally different from that displayed by the "fast-spiking" PVB-IR neurons.

In light of these differences, it is interesting to note that CB is coexpressed in large populations of PVB-IR neurons within the rodent neocortex, amygdala, and cerebellum (Celio, 1990;Kubota and Jones, 1993;Kubota et al., 1994;McDonald and Mascagni, 2001). Growing evidence indicates that, when coexpressed, CB and PVB may interact synergistically (Schwaller et al., 2002). For instance, dramatic changes relative to Purkinje cell dendritic spine morphology and densities were detected in double PVB-CB knockout mice but not in single PVB or CB knockouts (Vecellio et al., 2000). Similarly, the specific characteristics of synaptically evoked Ca^{2+} transients in Purkinjie cells were shown to depend on the coexpression of CB and PVB (Schmidt et al., 2003). It is also useful to remember that a role for CB in synaptic facilitation and consequent plasticity has been repeatedly shown (for review see Schwaller et al., 2002). Selective impairments in spatial learning paradigms and failure to maintain long-term potentiation in hippocampal neurons have been shown in transgenic mice deficient in CB (Molinari et al., 1996;Jouvenceau et al., 1999). Furthermore, CB, but not PVB, has also been shown to have neuroprotective effects (Orrenius and Nicotera, 1994;Yenari et al., 2001;D'Orlando et al., 2002). It is therefore possible that CB expression confers PVB-IR neurons with plastic and neuroprotective properties not shared by other PVB-IR neuronal subpopulations.

Our results show that approximately 25% of PVB-IR neurons in the human BLC-CO coexpress CB. These results are in apparent contradiction with a dual-antigen immunocytochemistry study in the rodent amygdala by McDonald and Betette (2001), reporting that 80% of PVB-IR neurons in the amygdala were found to coexpress CB. On the other hand, this estimate is consistent with reports describing the distribution of CB- and PVB-IR neurons in the human amygdala as complementary rather than overlapping (Sorvari et al., 1995,1996b). On a speculative level, such a contradiction may be explained by evidence suggesting an intriguing trend toward a decrease of PVB-CB coexpression in primate cortical or cortex-like regions compared with equivalent brain regions in rodents. For instance, substantial overlap of PVB and CB has been reported for the rodent neocortex (Kubota and Jones, 1993;Kubota et al., 1994), whereas virtually no coexpression of these two proteins was detected in the primate neocortex (Demeulemeester et al., 1989;Hendry et al., 1989;Hendry and Jones, 1991). If true, such a phylogenetic shift might reflect an evolving functional role played by neurons expressing PVB and/or CB in the cortex and amygdala.

Distribution of PVB-IR neuronal subpopulations within the human BLC-CO

The present study suggests that, at least in the human BLC-CO, PVB/PNN/–, and PVB/–/CB neurons are not only neurochemically different but also present distinct morphological features. Strikingly, most of the PVB/PNN/–and –/PNN/– neurons were LM cells, whereas virtually all PVB/–/CB and PVB/PNN/CB neurons were SB cells.

Overall, the evidence discussed so far indicates that PVB/PNN/– and PVB/–/CB neurons may represent two functionally and morphologically distinct subpopulations of PVB-IR neurons. Differences between these two subtypes of PVB-IR neurons are also reflected in their distribution within the BLC-CO (Fig. 8A). Our results in fact show that numbers of PVB/PNN/– neurons tend to increase sharply in the caudal portion of the BLC-CO, and more specifically within the LN, whereas PVB/–/CB show the opposite tendency, and the difference between these two slopes is statistically significant (Fig. 8A). Strikingly, these two main neuronal subgroups are also differentially distributed within BLC-CO nuclear subdivisions. The distribution of PVB/PNN/– neurons, along with the smaller population of PVB/PNN/CB neurons, was restricted to the ventrolateral subdivision of the LN and magnocellular

subdivision of the BN (Fig. 10). In contrast, the PVB/–/CB neurons were located mostly in the dorsal and intermediate divisions of the LN in the rostral half of the amygdala (Fig. 10).

Although the segregation within nuclear subregions is not absolute, these differences in distribution within the LN and BN are intriguing in light of the distinct patterns of connectivity of these regions. For instance, sensory inputs from the posterior thalamus, uni- and polysensory association cortices, and the orbital and medial prefrontal cortex have been reported to reach the dorsal portions of the LN, and particularly robust projections from the superior temporal gyrus innervate the ventral LN (Turner et al., 1980;Mufson et al., 1981;Yasui et al., 1987;Carmichael and Price, 1995;McDonald, 1998;Stefanacci and Amaral, 2002;Price, 2003). The dorsal LN sends a strong and nonreciprocal projection to the ventral LN, and these two LN subregions have different intraamygdala projections (Pitkanen and Kemppainen, 2002). Similarly, the magnocellular and parvicellular components of the BN have distinct connectivity profiles. For instance, the parvicellular BN has been reported to receive stronger inputs from the medial prefrontal cortex and the CA1/ prosubiculum region, whereas the magnocellular BN is more weakly innervated by these areas but receives inputs from the superior, middle, and inferior temporal gyri, carrying visual and auditory information (Saunders et al., 1988;Chiba et al., 2001;Stefanacci and Amaral, 2002). In light of these connections, it is tempting to speculate that PVB/–/CB neurons, located mainly in the dorsal LN, may be involved in the processing of a rather heterogeneous array of sensory information. On the other hand, the subgroups of PVB-IR neurons carrying PNNs (PVB/–PNN/–and PVB/PNN/CB), preferentially located in the ventral LN and magnocellular BN, are likely to affect processing of information originating from specialized cortical regions, such as the temporal gyrus, and to be involved in the integration of this information with the highly processed dorsal LN inputs.

CONCLUSIONS

In the human BLC-CO, subgroups of PVB-IR neurons can be distinguished on the basis of their expression of CB and presence of PNNs. Approximately 31% of PVB-IR neurons were enveloped in PNNs, while 18% of PVB-IR neurons expressed CB but did not possess PNNs. A small subgroup of PVB-IR neurons (7%) was labeled with both markers. The remaining 44% of PVB-IR neurons were negative for both CB and PNN. Each of these subgroups presented specific anatomical features with regard to the morphology and distribution within the BLC-CO. Interestingly, the PVB/PNN/– and PVB/–/CB subgroups of neurons showed the greatest differences. In consideration of the functional implications of these neurochemical markers and of the specific distributions of these neurons within the BLC-CO, we suggest that each of these distinct PVB-IR neuronal subgroups might contribute differentially to the information processing within the human amygdala.

Acknowledgements

Grant sponsor: National Institutes of Health; Grant number: MH066280 (to S.B.).

The authors are very grateful to Dr. Francine M. Benes for her thoughtful comments on the article.

LITERATURE CITED

Adolphs R, Tranel D, Damasio H, Damasio A. Impaired recognition of emotion in facial expressions following bilateral damage to the human amygdala. Nature 1994;372:669–672. [PubMed: 7990957]

Aggleton JP. The contribution of the amygdala to normal and abnormal emotional states. Trends Neurosci 1993;16:328–333. [PubMed: 7691009]

Amaral, DG.; Price, JL.; Pitkanen, A.; Carmichael, ST. Anatomical organization of the primate amygdaloid complex. In. In: Aggleton, JP., editor. The amygdala: neurobiological aspects of emotion, memory, and mental dysfunction. New York: Wiley-Liss; 1992.

Berretta S, Parthasarathy HP, Graybiel AM. Local release of GABAergic inhibition in the motor cortex induces immediate-early gene expression in indirect pathway neurons of the striatum. J Neu-rosci 1997;17:4752–4763.

Berridge MJ. Neuronal calcium signaling. Neuron 1998;21:13–26. [PubMed: 9697848]

Bignami A, Asher R, Perides G. The extracellular matrix of rat spinal cord: a comparative study on the localization of hyaluronic acid, glial hyaluronate-binding protein, and chondroitin sulfate proteoglycan. Exp Neurol 1992;117:90–93. [PubMed: 1377637]

Brothers LA. The social brain: a project for integrating primate behavior and neurophysiology in a new domain. Concepts Neurosci 1990;1:27–51.

Bruckner G, Brauer K, Hartig W, Wolff JR, Rickmann MJ, Derouiche A, Delpech B, Girard N, Oertel WH, Reichenbach A. Perineuronal nets provide a polyanionic, glia-associated form of microenvironment around certain neurons in many parts of the rat brain. Glia 1993;8:183–200. [PubMed: 7693589]

Caillard O, Moreno H, Schwaller B, Llano I, Celio MR, Marty A. Role of the calcium-binding protein parvalbumin in short-term synaptic plasticity. Proc Natl Acad Sci U S A 2000;97:13372–13377. [PubMed: 11069288]

Carmichael ST, Price JL. Limbic connections of the orbital and medial prefrontal cortex in macaque monkeys. J Comp Neurol 1995;363:615– 641. [PubMed: 8847421]

Cauli B, Audinat E, Lambolez B, Angulo MC, Ropert N, Tsuzuki K, Hestrin S, Rossier J. Molecular and physiological diversity of cortical nonpyramidal cells. J Neurosci 1997;17:3894 –3906. [PubMed: 9133407]

Celio MR. Calbindin D-28k and parvalbumin in the rat nervous system. Neuroscience 1990;35:375–475. [PubMed: 2199841]

Celio MR. Perineuronal nets of extracellular matrix around parvalbumin-containing neurons of the hippocampus. Hippocampus 1993;3:55–60. [PubMed: 8287112]

Celio MR, Blumcke I. Perineuronal nets—a specialized form of extracellular matrix in the adult nervous system. Brain Res Brain Res Rev 1994;19:128 –145. [PubMed: 8167657]

Celio MR, Spreafico R, De Biasi S, Vitellaro-Zuccarello L. Perineuronal nets: past and present. Trends Neurosci 1998;21:510 –515. [PubMed: 9881847]

Chard PS, Bleakman D, Christakos S, Fullmer CS, Miller RJ. Calcium buffering properties of calbindin D28k and parvalbumin in rat sensory neurones. J Physiol 1993;472:341–357. [PubMed: 8145149]

Chiba T, Kayahara T, Nakano K. Efferent projections of infralimbic and prelimbic areas of the medial prefrontal cortex in the Japanese monkey, Macaca fuscata. Brain Res 2001;888:83–101. [PubMed: 11146055]

D'Orlando C, Celio MR, Schwaller B. Calretinin and calbindin D-28k, but not parvalbumin protect against glutamate-induced delayed excitotoxicity in transfected N18-RE 105 neuroblastoma-retina hybrid cells. Brain Res 2002;945:181–190. [PubMed: 12126880]

DeFelipe J, Hendry SH, Jones EG. Visualization of chandelier cell axons by parvalbumin immunoreactivity in monkey cerebral cortex. Proc Natl Acad Sci U S A 1989;86:2093–2097. [PubMed: 2648389]

Demeulemeester H, Vandesande F, Orban GA, Heizmann CW, Pochet R. Calbindin D-28K and parvalbumin immunoreactivity is confined to two sep arate neuronal subpopulations in the cat visual cortex, whereas partial coexistence is shown in the dorsal lateral geniculate nucleus. Neurosci Lett 1989;99:6–11. [PubMed: 2748019]

Fonseca M, Soriano E, Ferrer I, Martinez A, Tunon T. Chandelier cell axons identified by parvalbumin-immunoreactivity in the normal human temporal cortex and in Alzheimer's disease. Neuroscience 1993;55:1107–1116. [PubMed: 8232900]

Freund TF, Buzsaki G. Interneurons of the hippocampus. Hippocampus 1996;6:347–470. [PubMed: 8915675]

Gabbott P, Bacon S. Local circuit neurons in the medial prefrontal cortex (areas 24a,b,c, 25 and 32) in the monkey: I. Cell morphology and morphometrics. J Comp Neurol 1996;364:567– 608. [PubMed: 8821449]

Gan L, Kaczmarek LK. When, where, and how much? Expression of the Kv3.1 potassium channel in high-frequency firing neurons. J Neurobiol 1998;37:69–79. [PubMed: 9777733]

Gloor, P. Role of the human limbic system in perception, memory and affect. In. In: Doane, BK.; Livingston, KE., editors. The limbic system . New York: Raven Press ; 1986. p. 159 -169.

Gloor, P. The temporal lobe and limbic system. New York: Oxford University Press; 1997. The amygdaloid system; p. 591-721.

Halgren, E. Emotional neurophysiology and the amygdala within the context of human cognition. In. In: Aggleton, JP., editor. The amygdala. New York: Wiley-Liss; 1992. p. 191-228.

Hartig W, Brauer K, Bruckner G. Wisteria floribunda agglutinin-labelled nets surround parvalbumin-containing neurons. Neuroreport 1992;3:869–872. [PubMed: 1421090]

Hartig W, Brauer K, Bigl V, Bruckner G. Chondroitin sulfate proteoglycan-immunoreactivity of lectin-labeled perineuronal nets around parvalbumin-containing neurons. Brain Res 1994;635:307–311. [PubMed: 8173967]

Hartig W, Bruckner G, Brauer K, Schmidt C, Bigl V. Allocation of perineuronal nets and parvalbumin-, calbindin- D28k- and glutamic acid decarboxylase-immunoreactivity in the amygdala of the rhesus monkey. Brain Res 1995;698:265–269. [PubMed: 8581495]

Hartig W, Derouiche A, Welt K, Brauer K, Grosche J, Mader M, Reichen-bach A, Bruckner G. Cortical neurons immunoreactive for the potassium channel Kv3.1b subunit are predominantly surrounded by perineuronal nets presumed as a buffering system for cations. Brain Res 1999;842:15–29. [PubMed: 10526091]

Hendry SH, Jones EG. GABA neuronal subpopulations in cat primary auditory cortex: co-localization with calcium binding proteins. Brain Res 1991;543:45–55. [PubMed: 2054675]

Hendry SH, Jones EG, Emson PC, Lawson DE, Heizmann CW, Streit P. Two classes of cortical GABA neurons defined by differential calcium binding protein immunoreactivities. Exp Brain Res 1989;76:467–472. [PubMed: 2767197]

Hockfield S, Kalb RG. Activity-dependent structural changes during neuronal development. Curr Opin Neurobiol 1993;3:87–92. [PubMed: 8453296]

Horn AK, Bruckner G, Hartig W, Messoudi A. Saccadic omnipause and burst neurons in monkey and human are ensheathed by perineuronal nets but differ in their expression of calcium-binding proteins. J Comp Neurol 2003;455:341–352. [PubMed: 12483686]

Jouvenceau A, Potier B, Battini R, Ferrari S, Dutar P, Billard JM. Glutamatergic synaptic responses and long-term potentiation are impaired in the CA1 hippocampal area of calbindin D(28k)-deficient mice. Synapse 1999;33:172–180. [PubMed: 10420165]

Kawaguchi Y, Kubota Y. Correlation of physiological subgroupings of nonpyramidal cells with parvalbumin- and calbindin D28k-immunoreactive neurons in layer V of rat frontal cortex. J Neurophysiol 1993;70:387–396. [PubMed: 8395585]

Kawaguchi, Y.; Kubota, Y. Local circuit neurons in the frontal cortex and the neostriatum. In. In: Kimura, M.; Graybiel, AM., editors. Functions of the corticobasal ganglia loop. Tokyo: Springer-Verlag; 1995.

Kemppainen S, Pitkanen A. Distribution of parvalbumin, calretinin, and calbindin-D(28k) immunoreactivity in the rat amygdaloid complex and colocalization with gamma-aminobutyric acid. J Comp Neurol 2000;426:441–467. [PubMed: 10992249]

Kosaka T, Heizmann CW. Selective staining of a population of parvalbumin-containing GABAergic neurons in the rat cerebral cortex by lectins with specific affinity for terminal N-acetylgalactosamine. Brain Res 1989;483:158 –163. [PubMed: 2565147]

Kubota Y, Jones EG. Co-localization of two calcium binding proteins in GABA cells of rat piriform cortex. Brain Res 1993;600:339–344. [PubMed: 8435756]

Kubota Y, Hattori R, Yui Y. Three distinct subpopulations of GABAergic neurons in rat frontal agranular cortex. Brain Res 1994;649:159 –173. [PubMed: 7525007]

Lander C, Kind P, Maleski M, Hockfield S. A family of activity-dependent neuronal cell-surface chondroitin sulfate proteoglycans in cat visual cortex. J Neurosci 1997;17:1928 –1939. [PubMed: 9045722]

LeDoux, JE. Emotion and the amygdala . In: Aggleton, JP., editor. The amygdala. New York: Wiley-Liss; 1992. p. 339 -351.

Lee SH, Rosenmund C, Schwaller B, Neher E. Differences in Ca^{2+} buffering properties between excitatory and inhibitory hippocampal neurons from the rat. J Physiol 2000;525:405– 418. [PubMed: 10835043]

Lenz S, Perney TM, Qin Y, Robbins E, Chesselet MF. GABA-ergic interneurons of the striatum express the Shaw-like potassium channel Kv3.1. Synapse 1994;18:55– 66. [PubMed: 7825124]

Luth HJ, Fischer J, Celio MR. Soybean lectin binding neurons in the visual cortex of the rat contain parvalbumin and are covered by glial nets. J Neurocytol 1992;21:211–221. [PubMed: 1560253]

Mai, JK.; Assheuer, J.; Paxinos, G. Atlas of the human brain. San Diego: Academic Press; 1997.

McDonald AJ. Cortical pathways to the mammalian amygdala. Prog Neurobiol 1998;55:257–332. [PubMed: 9643556]

McDonald AJ, Betette RL. Parvalbumin-containing neurons in the rat basolateral amygdala: morphology and co-localization of calbindin-D(28k). Neuroscience 2001;102:413–425. [PubMed: 11166127]

McDonald AJ, Mascagni F. Colocalization of calcium-binding proteins and GABA in neurons of the rat basolateral amygdala. Neuroscience 2001;105:681–693. [PubMed: 11516833]

McDonald AJ, Mascagni F. Parvalbumin-containing interneurons in the basolateral amygdala express high levels of the alpha1 subunit of the GABAA receptor. J Comp Neurol 2004;473:137–146. [PubMed: 15067724]

McDonald AJ, Mascagni F, Mania I, Rainnie DG. Evidence for a perisomatic innervation of parvalbumin-containing interneurons by individual pyramidal cells in the basolateral amygdala. Brain Res 2005;1035:32–40. [PubMed: 15713274]

Mikkonen M, Soininen H, Pitkanen A. Distribution of parvalbumin-, calretinin-, and calbindin-D28k-immunoreactive neurons and fibers in the human entorhinal cortex. J Comp Neurol 1997;388:64–88. [PubMed: 9364239]

Molinari S, Battini R, Ferrari S, Pozzi L, Killcross AS, Robbins TW, Jouvenceau A, Billard JM, Dutar P, Lamour Y, Baker WA, Cox H, Emson PC. Deficits in memory and hippocampal long-term potentiation in mice with reduced calbindin D28K expression. Proc Natl Acad Sci U S A 1996;93:8028–8033. [PubMed: 8755597]

Morawski M, Bruckner MK, Riederer P, Bruckner G, Arendt T. Perineuronal nets potentially protect against oxidative stress. Exp Neurol 2004;188:309–315. [PubMed: 15246831]

Morris NP, Henderson Z. Perineuronal nets ensheath fast spiking, parvalbumin-immunoreactive neurons in the medial septum/diagonal band complex. Eur J Neurosci 2000;12:828–838. [PubMed: 10762312]

Mufson EJ, Mesulam M-M, Pandya DN. Insular interconnections with the amygdala in the rhesus monkey. Neuroscience 1981;6:1231–1248. [PubMed: 6167896]

Muller JF, Mascagni F, McDonald AJ. Coupled networks of parvalbumin-immunoreactive interneurons in the rat basolateral amygdala . J Neurosci 2005;25:7366 –7376. [PubMed: 16093387]

Murakami T, Ohtsuka A. Perisynaptic barrier of proteoglycans in the mature brain and spinal cord. Arch Histol Cytol 2003;66:195–207. [PubMed: 14527161]

Orrenius S, Nicotera P. The calcium ion and cell death. J Neural Transm Suppl 1994;43:1–11. [PubMed: 7884392]

Pape HC, Par D, Driesang RB. Two types of intrinsic oscillations in neurons of the lateral and basolateral nuclei of the amygdala. J Neurophysiol 1998;79:205–216. [PubMed: 9425192]

Paré D, Gaudreau H. Projection cells and interneurons of the lateral and basolateral amygdala: distinct firing patterns and differential relation to theta and delta rhythms in conscious cats. J Neurosci 1996;16:3334–3350. [PubMed: 8627370]

Paré D, Collins DR, Pelletier JG. Amygdala oscillations and the consolidation of emotional memories. Trends Cogn Sci 2002;6:306 –314. [PubMed: 12110364]

Perney TM, Marshall J, Martin KA, Hockfield S, Kaczmarek LK. Expression of the mRNAs for the Kv3.1 potassium channel gene in the adult and developing rat brain. J Neurophysiol 1992;68:756–766. [PubMed: 1432046]

Pitkanen A, Kemppainen S. Comparison of the distribution of calcium-binding proteins and intrinsic connectivity in the lateral nucleus of the rat, monkey, and human amygdala. Pharmacol Biochem Behav 2002;71:369–377. [PubMed: 11830171]

Price JL. Comparative aspects of amygdala connectivity. Ann N YAcad Sci 2003;985:50–58.

Rainnie DG, Asprodini EK, Shinnick Gallagher P. Inhibitory transmission in the basolateral amygdala. J Neurophysiol 1991;66:999–1009. [PubMed: 1684384]

Rhodes KE, Fawcett JW. Chondroitin sulphate proteoglycans: preventing plasticity or protecting the CNS? J Anat 2004;204:33– 48. [PubMed: 14690476]

Saunders RC, Rosene DL, Van Hoesen GW. Comparison of the efferents of the amygdala and the hippocampal formation in the rhesus monkey: II. Reciprocal and non-reciprocal connections. J Comp Neurol 1988;271:185–207. [PubMed: 2454247]

Schmidt H, Stiefel KM, Racay P, Schwaller B, Eilers J. Mutational analysis of dendritic Ca^{2+} kinetics in rodent Purkinje cells: role of parvalbumin and calbindin D28k. J Physiol 2003;551:13–32. [PubMed: 12813159]

Schnell SA, Staines WA, Wessendorf MW. Reduction of lipofuscin-like autofluorescence in fluorescently labeled tissue. J Histochem Cytochem 1999;47:719–730. [PubMed: 10330448]

Schwaller B, Meyer M, Schiffmann S. "New" functions for "old" proteins: the role of the calcium-binding proteins calbindin D-28k, calretinin and parvalbumin, in cerebellar physiology. Studies with knockout mice. Cerebellum 2002;1:241–258. [PubMed: 12879963]

Seeger G, Luth HJ, Winkelmann E, Brauer K. Distribution patterns of Wisteria floribunda agglutinin binding sites and parvalbumin-immunoreactive neurons in the human visual cortex: a double-labelling study. J Hirnforsch 1996;37:351–366. [PubMed: 8872558]

Sekirnjak C, Martone ME, Weiser M, Deerinck T, Bueno E, Rudy B, Ellisman M. Subcellular localization of the K^+ channel subunit Kv3.1b in selected rat CNS neurons. Brain Res 1997;766:173–17. [PubMed: 9359601]

Sims KS, Williams RS. The human amygdaloid complex: a cytologic and histochemical atlas using Nissl, myelin, acetylcholinesterase and nicotinamide adenine dinucleotide phosphate diaphorase staining. Neuroscience 1990;36:449–472. [PubMed: 1699167]

Smith Y, Pare JF, Pare D. Cat intraamygdaloid inhibitory network: ultrastructural organization of parvalbumin-immunoreactive elements. J Comp Neurol 1998;391:164–179. [PubMed: 9518267]

Smith Y, Pare JF, Pare D. Differential innervation of parvalbumin-immunoreactive interneurons of the basolateral amygdaloid complex by cortical and intrinsic inputs. J Comp Neurol 2000;416:496–508. [PubMed: 10660880]

Sorvari H, Soininen H, Paljarvi L, Karkola K, Pitkanen A. Distribution of parvalbumin-immunoreactive cells and fibers in the human amygdaloid complex. J Comp Neurol 1995;360:185–212. [PubMed: 8522643]

Sorvari H, Miettinen R, Soininen H, Pitkanen A. Parvalbumin-immunoreactive neurons make inhibitory synapses on pyramidal cells in the human amygdala: a light and electron microscopic study. Neurosci Lett 1996a;217:93–96. [PubMed: 8916080]

Sorvari H, Soininen H, Pitkanen A. Calbindin-D28K-immunoreactive cells and fibres in the human amygdaloid complex. Neuroscience 1996b ;75:421– 443. [PubMed: 8931007]

Stefanacci L, Amaral DG. Some observations on cortical inputs to the macaque monkey amygdala: an anterograde tracing study. J Comp Neurol 2002;451:301–323. [PubMed: 12210126]

Turner B, Mishkin M, Knapp M. Organization of the amygdalopetal projections from modality-specific cortical association areas in the monkey. J Comp Neurol 1980;191:515–543. [PubMed: 7419732]

Vecellio M, Schwaller B, Meyer M, Hunziker W, Celio MR. Alterations in Purkinje cell spines of calbindin D-28 k and parvalbumin knock-out mice. Eur J Neurosci 2000;12:945–954. [PubMed: 10762324]

Vreugdenhil M, Jefferys JG, Celio MR, Schwaller B. Parvalbumin-deficiency facilitates repetitive IPSCs and gamma oscillations in the hippocampus. J Neurophysiol 2003;89:1414–1422. [PubMed: 12626620]

Wegner F, Hartig W, Bringmann A, Grosche J, Wohlfarth K, Zuschratter W, Bruckner G. Diffuse perineuronal nets and modified pyramidal cells immunoreactive for glutamate and the GABA(A) receptor alpha1 subunit form a unique entity in rat cerebral cortex. Exp Neurol 2003;184:705–714. [PubMed: 14769362]

Weiser M, Bueno E, Sekirnjak C, Martone ME, Baker H, Hillman D, Chen S, Thornhill W, Ellisman M, Rudy B. The potassium channel subunit KV3.1b is localized to somatic and axonal membranes of specific populations of CNS neurons. J Neurosci 1995;15:4298–4314. [PubMed: 7790912]

Yamaguchi Y. Lecticans: organizers of the brain extracellular matrix. Cell Mol Life Sci 2000;57:276–289. [PubMed: 10766023]

Yasui Y, Itoh K, Sugimoto T, Mizuno N. Thalamocortical and thalamo-amygdaloid projections from the parvicellular division of the posteromedial ventral nucleus in the cat. J Comp Neurol 1987;257:253–268. [PubMed: 3571528]

Yenari MA, Minami M, Sun GH, Meier TJ, Kunis DM, McLaughlin JR, Ho DY, Sapolsky RM, Steinberg GK. Calbindin d28k overexpression protects striatal neurons from transient focal cerebral ischemia. Stroke 2001;32:1028–1035. [PubMed: 11283407]

Zaitsev AV, Gonzalez-Burgos G, Povysheva NV, Kroner S, Lewis DA, Krimer LS. Localization of calcium-binding proteins in physiologically and morphologically characterized interneurons of monkey dorsolateral prefrontal cortex. Cereb Cortex 2005;15:1178–1186. [PubMed: 15590911]

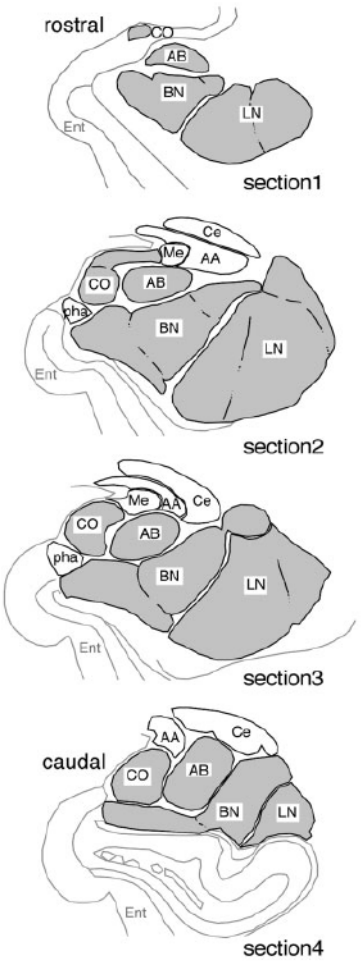

Fig 1.

Diagrams representing coronal sections through the amygdala chosen as standards for quantification of PVB-IR neurons in the BLC-CO. In this study, neurons were counted in four representative coronal sections of the amygdala in each of five normal subjects. The diagrams shown here from rostral (section 1) to caudal (section 4) were used as standards for selecting such sections so that each rostrocaudal level could be closely matched across cases. These sections were chosen to maximize the number of PVB-IR detected. Nuclei included in the BLC-CO definition are filled in gray. AA, anterior amygdaloid area; AB, accessory basal nucleus; BN, basal nucleus; Ce, central nucleus; CO, cortical nucleus; Ent, entorhinal cortex; LN, lateral nucleus; Me, medial nucleus; pha, parahippocampalamygdaloid transitional area (modified from Mai et al., 1997).

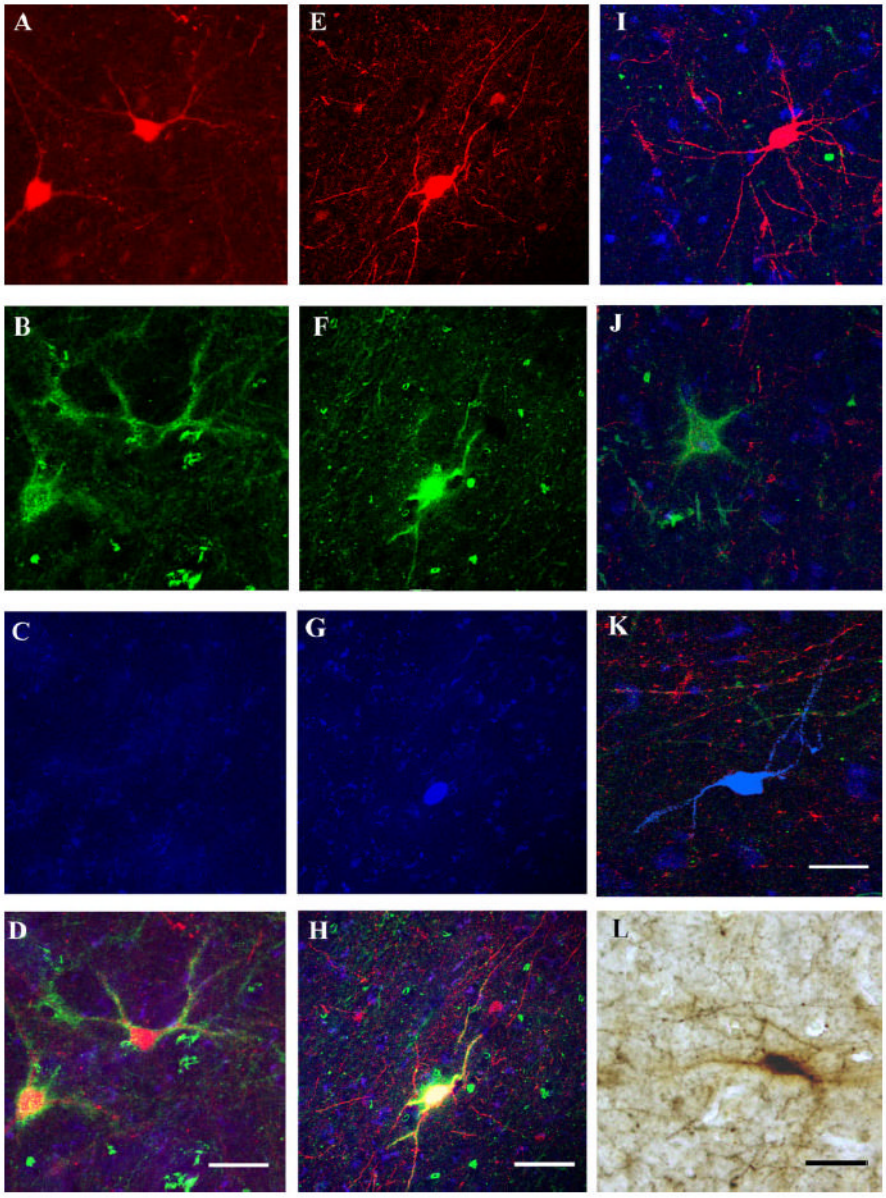

Fig 2.

Photomicrographs showing examples of immunoreactive neurons in the LN. **A–K** show confocal microphotomicrographs; pseudocolors were red for PVB, green for PNN, and blue for CB. A–D show two PVB/PNN/– neurons. These neurons were found to express PVB (A) and to be surrounded by a PNN (B), but they were not IR for CB (C). D displays the overlay of the three markers. The pseudocolor yellow represents overlap between the red and the green. E–H illustrate a PVB/PNN/CB neuron. This neuron was demonstrated to express PVB (E) and CB (G) and to be wrapped by a PNN (F). E–G are shown superimposed in H to confirm the colocalization of the three markers (pseudocolor white). I–K show examples of neurons exclusively IR for PVB, PNN, and CB, respectively. Note that these microphotographs are overlays of the three channels, so that cell bodies and neuropil IR for each of the three markers are visible in the background. **L** shows a light microscopic photomicrograph of a PVB-IR neuron (black) surrounded by a PNN (brown). Scale bars = 100 μm in D (applies to A–D), H (applies to E–H), L (applies to I–L).

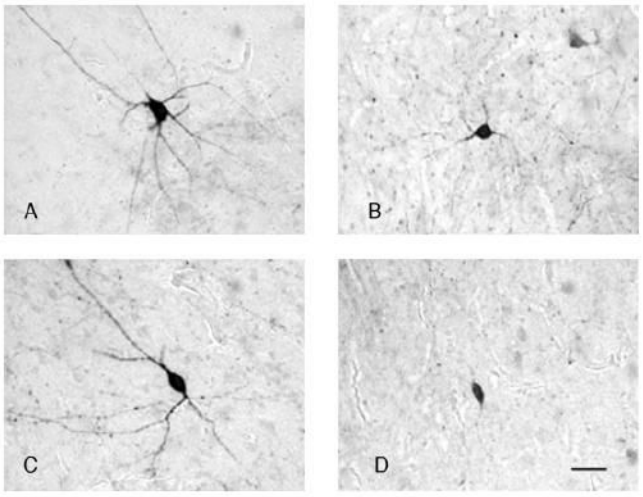

Fig 3.

Examples of four morphological types of PVB-IR neurons in the LN. Light microscopy photomicrographs of PVB-IR neurons belonging to each of the four morphological categories identified in this study. **A** and **B** show examples of large and small multipolar neurons, respectively. These neurons had irregularly shaped or rounded somata and several primary dendrites emerging in various directions. **C** and **D** show examples of large and small bipolar neurons, respectively. Note the fusiform shape of the somata and the two primary dendrites emerging at the opposite poles. Scale bar =30 μm in D (applies to A–D).

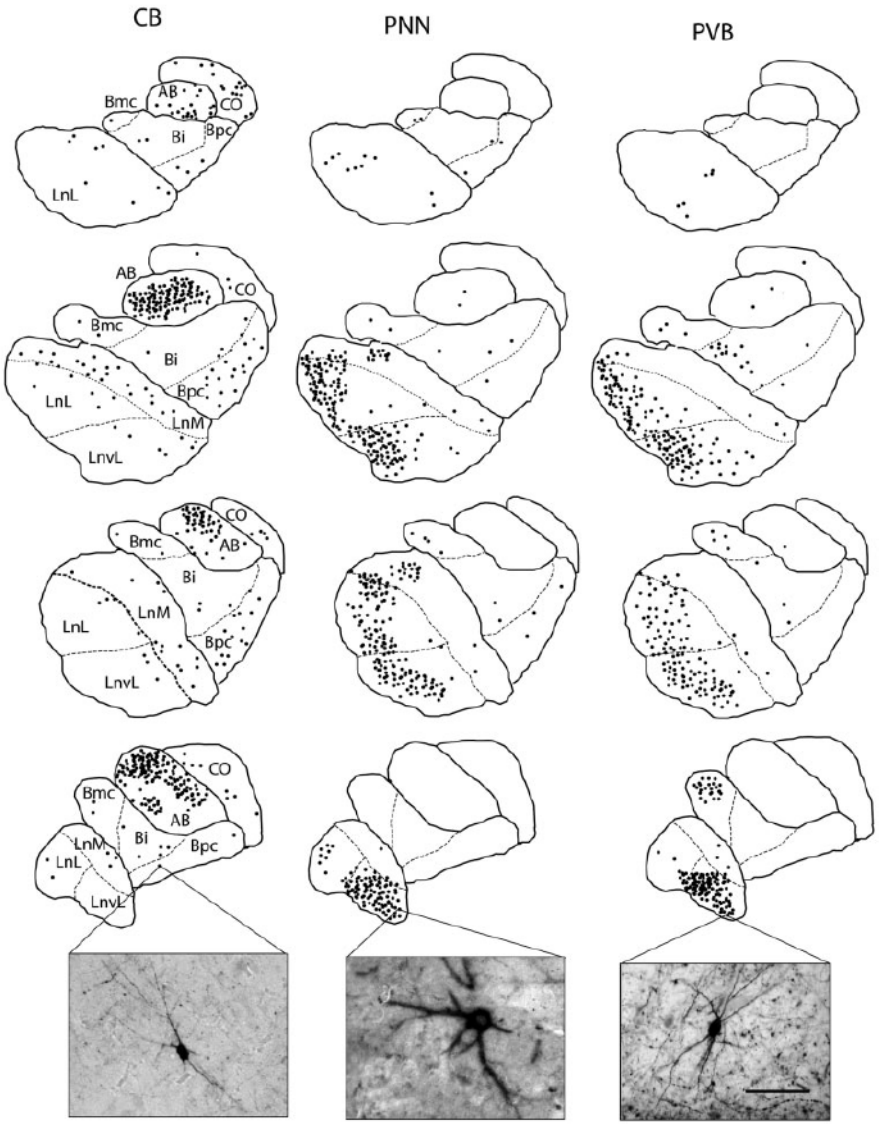

Fig 4.

Plots and photomicrographs of CB-IR neurons, PNN, and PVB-IR neurons within the LN, BN, AB, and CO. In order to show, and compare, the distribution of CB- and PVB-IR neurons and PNNs in the human amygdala, 40-μm-thick adjacent sections from one of the five subjects included in this study were immunostained for CB, PVB, and PNN by using a nickel-enhanced diaminobenzidine protocol. Plots were made via computer-assisted light microscopy (Bioquant Nova Prime v6.0; R&M Biometrics Inc.). Sections are displayed in rostrocaudal order (upper to lower). Each dot represents a neuron. CB-IR neurons were found to be scattered throughout the BLC-CO, with the AB showing by far the highest numbers. PVB-IR neurons and PNNs were found mostly in the lateral and ventrolateral subdivisions of the LN and, to a lesser extent, in the magnocellular subdivision of the BN. Note the large degree of overlap in the distribution of these two latter markers. Bi, basal nucleus intermediate; Bmc, basal nucleus magnocellular subdivision; Bpc, basal nucleus, parvicellular subdivision; LnL, lateral nucleus lateral subdivision; LnM, lateral nucleus medial subdivision; LnvL, lateral nucleus ventrolateral subdivision. Scale bar = 120μm (applies to all photomicrographs).

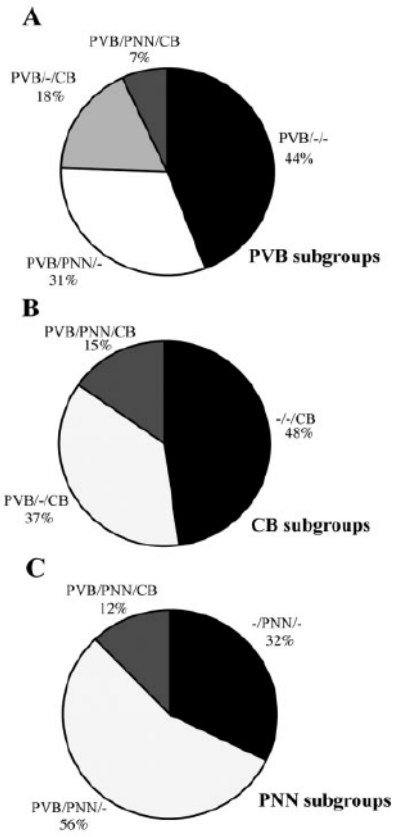

Fig 5.

Pie charts representing the percentages of each neuronal subpopulation identified within the BLC-CO. Among PVB-IR neurons, the two largest subgroups were represented by PVB/PNN/– and PVB/–/–neurons. Interestingly, PVB/PNN/CB neurons represented the smallest population, whether considered as percentages of PVB (**A**), CB (**B**), or PNN (**C**). It is also worth noting that –/PNN/CB neurons were not detected.

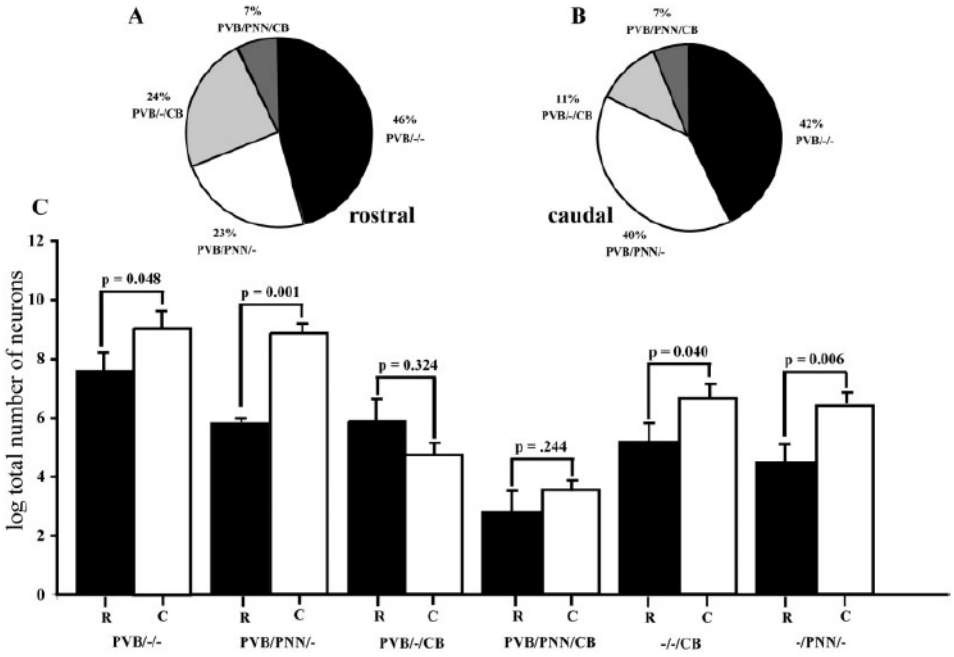

Fig 6.

Percentage distributions and neuron numbers of subgroups of PVB-IR neurons vary across a rostrocaudal gradient. In **A** and **B**, subgroups of neurons are shown as percentages of the entire population of PVB-IR neurons counted in the BLC-CO (four sections/ case; five cases). Data from the rostral (sections 1, 2; A) and the caudal (sections 3, 4; B) portions of the BLC-CO are represented separately to show changes within the rostrocaudal gradient. These changes aredue in great part to an increase of the percentage of PVB/PNN/–neurons in caudal portion at the expense of PVB/–/CB neurons. In **C**, bar graphs show comparisons between total numbers of cells (logarithmic transformation) for each neuronal subgroup detected in the rostral and caudal portion of the BLC-CO. Numbers of PVB/–/–, PVB/PNN/–, –/–/CB, and –/PNN/– neurons were significantly higher in the caudal portion.

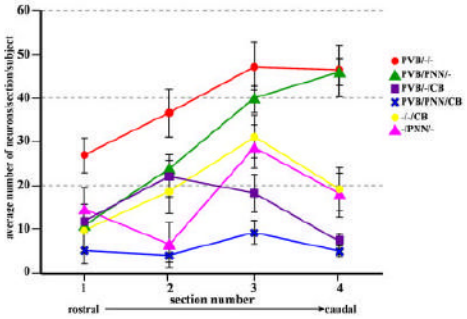

Fig 7.

Distribution of neuronal subgroups along the rostrocaudal axis of the BLC-CO. Numbers of cells for each neuronal subgroup examined were plotted for each of the four sections included in the analysis to show their rostrocaudal distribution. Numbers of neurons were averaged across subjects (error bars represent SEM). In the BLC-CO, numbers of PVB/PNN/– and PVB/–/– neurons progressively increase in more caudal sections, whereas numbers of PVB/–/CB show the opposite tendency. [Color figure can be viewed in the online issue, which is available at www.interscience.wiley.com.]

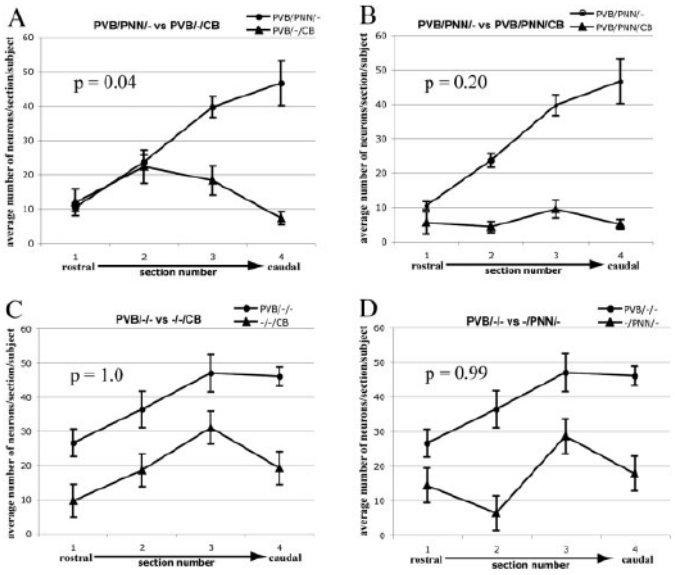

Fig 8.

Comparisons between distribution slopes of subgroups of IR neurons. Numbers of neurons counted in each of the four sections analyzed were averaged across cases. Paired *t*-tests, corrected for multiple comparisons, were used to test whether the rostrocaudal distribution slopes of pairs of neuron subgroups were significantly different. Numbers of PVB/PNN/– neurons sharply increased in the caudal portion of the BLC-CO (sections 3, 4), whereas PVB/–/CB neurons showed a decrease. The distribution slopes of these two neuron subgroups were found to be significantly different ($P=0.04$; **A**). The distributions of the other pairs considered did not show significant differences (**B–D**).

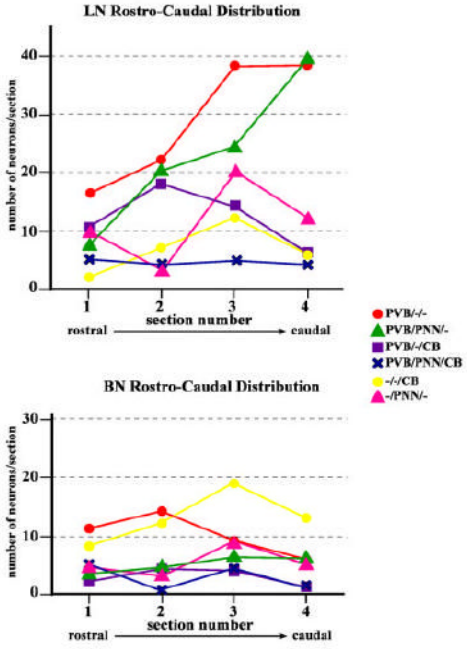

Fig 9.

Distribution of neuronal subgroups along the rostrocaudal axis of the LN and BN. In one representative amygdala, numbers of cells for each neuronal subgroup were plotted for each of the four sections included in the analysis to show their rostrocaudal distribution. In the LN, numbers of PVB/PNN/– and PVB/–/– neurons progressively increased in more caudal sections, whereas numbers of PVB/–/CB showed the opposite tendency. These distribution patterns were not detected in the BN, suggesting that rostrocaudal gradients detected in the BLC-CO may be driven mainly by the LN. [Color figurecan be viewed in the online issue, which is available at www.interscience.wiley.com.]

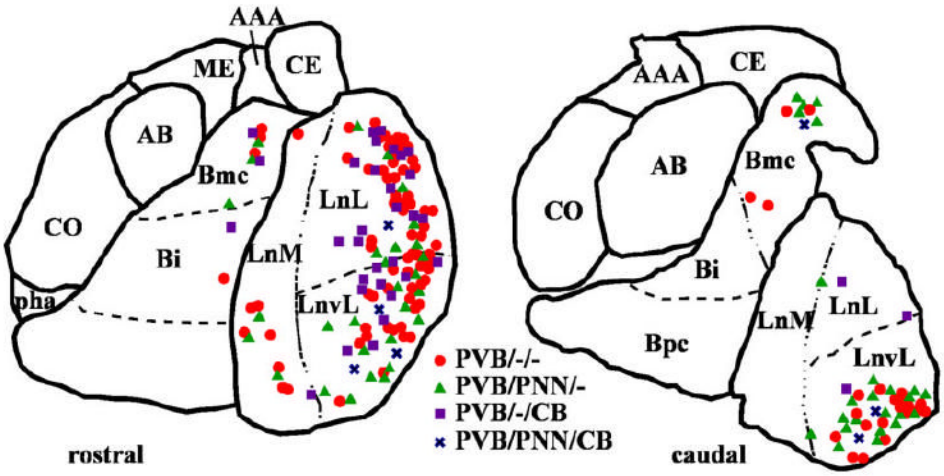

Fig 10.

Observed distribution of four subgroups of PVB-IR neurons within two coronal planes of the human amygdala. Neurons were plotted from one of the five amygdalas included in the study. In the rostral plane (compare with section 2 in Fig. 1), PVB/PNN/– and PVB/PNN/CB neurons were found mostly in the ventrolateral portion of LN, whereas most PVB/–/CB and PVB/–/– were detected in the lateral LN. The magnocellular portion of the BN contained mainly PVB/–/– and PVB/PNN/– neurons. In more caudal planes (compare with section 4 in Fig. 1), PVB/PNN/–, PVB/PNN/CB, and PVB/–/–neurons were strictly confined to the ventrolateral subdivision of the LN, and fewer PVB/–/CB were found in its lateral subdivision. [Color figure can be viewed in the online issue, which is available at www.interscience.wiley.com.]

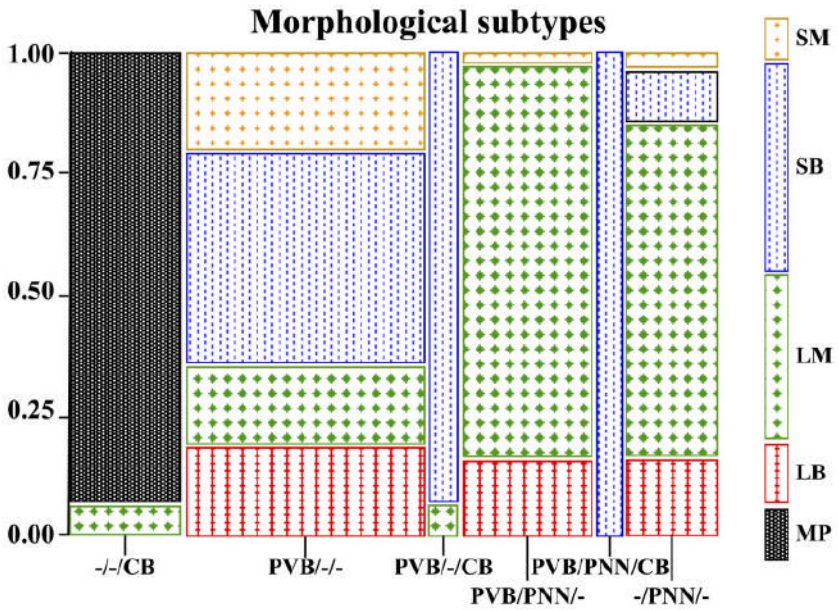

Fig 11.

Contingency table representing the morphological subtypes for each amygdalar neuronal subpopulation included in the study. Specific neurochemical subgroups were strongly associated with distinct morphological phenotypes (Chi-squre $P=0.0001$). Strikingly, neurons possessing PNNs showed a strong tendency to be large and multipolar, with the conspicuous exception of PVB/PNN/CB neurons, which were all small bipolar cells. Consistently, PVB/–/CB neurons also were mostly small fusiform. LB, large bipolar; LM, large multipolar; MP, multipolar; SB, small bipolar; SM, small multipolar. [Color figure can be viewed in the online issue, which is available at www.interscience.wiley.com.]

TABLE 1

Demographic and Descriptive Data of the Sample

Case No.	Age (years)	PMI	Sex	Hemisphere
B4585	59	21.5	Male	Left
B4586	37	18.8	Male	Right
B4595	65	17.3	Male	Left
B4625	53	24.0	Female	Right
B4725	58	17.8	Female	Right
Average	54.4	19.8	3M/2F	2L/3R

TABLE 2

Paired *t*-Test Analysis of the Rostrocaudal Distribution Slopes of Each Neuronal Subpopulation

	Paired *t*-test comparisons of slopes				
Marker comparison	**Mean differences**	**SE**	***t* value**	**Correlation**	***P* value**
PVB/-/- vs. PVB/PNN/–	0.59	0.13	4.47	0.05	0.17
PVB/-/- vs. PVB/-/CB	–0.90	0.28	–3.20	0.11	0.49
PVB/-/- vs. PVB/PNN/CB	-0.36	0.28	-1.31	0.25	1.00
PVB/-/- vs. –/–/CB	-0.09	0.23	-0.37	-0.16	1.00
PVB/-/- vs. -/PNN/-	-0.14	0.28	-0.51	-0.67	1.00
PVB/PNN/- vs. PVB/-/CB	-1.50	0.23	-6.43	0.66	0.04[1]
PVB/PNN/- vs. PVB/PNN/CB	-0.96	0.23	-4.13	0.85	0.22
PVB/PNN/- vs. -/-/CB	-0.68	0.22	-3.15	-0.44	0.51
PVB/PNN/- vs. -/PNN/-	-0.73	0.17	-4.33	0.35	0.18
PVB/-/CB vs. PVB/PNN/CB	0.54	0.23	2.36	0.67	1.00
PVB/-/CB vs. -/-/CB	0.81	0.44	1.85	30.91	1.00
PVB/-/CB vs. -/PNN/-	0.76	0.21	3.60	0.62	0.34
PVB/PNN/CB vs. -/-/CB	0.28	0.42	0.66	-0.65	1.00
PVB/PNN/CB vs. -/PNN/-	0.22	0.32	0.70	0.10	1.00
-/-/CB vs. -/PNN/-	-0.05	0.31	-0.17	-0.45	1.00

[1] Statistically significant at $P = 0.05$ after Bonferroni correction multiple comparisons.

TABLE 3

Paired *t*-Test Analysis of the Total Number of Neurons in Each Neuronal Subpopulation

	Paired *t*-test total numbers				
Marker comparison	**Mean differences**	**SE**	***t* value**	**Correlation**	***P* value**
Rostral					
PVB–/– vs. PVB/PNN/–	-1.800	0.63	-2.880	-0.57	0.68
PVB/-/- vs. PVB/-/CB	-1.801	0.87	-2.080	0.08	1.00
PVB/-/- vs. PVB/PNN/CB	-4.812	1.06	-4.530	-0.57	0.17
PVB/-/- vs. -/-/CB	-2.444	0.40	-6.074	0.75	0.06
PVB/-/- vs. -/PNN/-	-3.194	0.70	-4.541	0.16	0.17
PVB/PNN/- vs. PVB/-/CB	0.001	0.81	0.001	-0.77	1.00
PVB/PNN/- vs. PVB/PNN/CB	-3.010	0.69	-4.353	-0.35	0.18
PVB/PNN/- vs. -/-/CB	-0.642	0.61	-1.064	-0.20	1.00
PVB/PNN/- vs. -/PNN/-	-1.390	0.59	-2.372	-0.39	1.00
PVB/-/CB vs. PVB/PNN/CB	-3.011	0.54	-5.593	0.69	0.08
PVB/-/CB vs. -/-/CB	-0.643	0.89	-0.734	0.07	1.00
PVB/-/CB vs. -/PNN/-	-1.393	0.47	-2.973	0.75	0.62
PVB/PNN/CB vs. -/-/CB	2.370	1.10	2.142	-0.64	1.00
PVB/PNN/CB vs. -/PNN/-	1.624	0.74	2.190	0.23	1.00
-/-/CB vs. -/PNN/-	-0.751	0.53	-1.412	0.54	1.00
Caudal					
PVB/-/- vs. PVB/PNN/-	-0.21	0.35	-0.59	0.89	1.000
PVB/-/- vs. PVB/-/CB	-4.58	0.37	-12.85	0.87	0.003[1]
PVB/-/- vs. PVB/PNN/CB	-5.84	0.64	-9.10	0.22	0.012[1]
PVB/-/- vs. -/-/CB	-2.55	0.41	-6.29	0.76	0.049[1]
PVB/-/- vs. -/PNN/-	-2.79	0.33	-8.54	0.93	0.015[1]
PVB/PNN/- vs. PVB/-/CB	-4.38	0.23	-19.40	0.80	0.002[1]
PVB/PNN/- vs. PVB/PNN/CB	-5.63	0.31	-18.17	0.60	0.002[1]
PVB/PNN/- vs. -/-/CB	-2.34	0.24	-9.75	0.87	0.009[1]
PVB/PNN/- vs. -/PNN/-	-2.59	0.10	-26.47	0.96	0.002[1]
PVB/-/CB vs. PVB/PNN/CB	-1.26	0.46	-2.73	0.13	0.795
PVB/-/CB vs. -/-/CB	2.03	0.33	6.17	0.72	0.053
PVB/-/CB vs. -/PNN/-	1.79	0.13	13.52	0.93	0.003[1]
PVB/PNN/CB vs. -/-/CB	3.29	0.34	9.75	0.70	0.009[1]
PVB/PNN/CB vs. -/PNN/-	3.05	0.36	8.38	0.43	0.017[1]
-/-/CB vs. -/PNN/-	-0.24	0.24	-1.02	0.88	1.000

[1] Statistically significant at $P = 0.05$ after Bonferroni correction for correlated multiple comparisons.